

## **AN INVESTIGATION OF PULSATILE BLOOD FLOW IN A BIFURCATION ARTERY USING A GRID-FREE METHOD**

**Matthew SINNOTT<sup>1</sup>, Paul W. CLEARY<sup>1</sup> and Mahesh PRAKASH<sup>1</sup>**

<sup>1</sup> CSIRO Minerals, Clayton, Victoria 3169, AUSTRALIA

### **ABSTRACT**

CFD modelling is a powerful, but largely under-utilised tool for biomedical applications. In particular, it has great potential for helping us better understand the mechanisms responsible for cardiovascular disease such as atherosclerosis and thrombi formation. Flow behaviour in blood vessels has been shown to depend strongly on features of the local geometry such as branching, bending, and regions of flow constriction. The simplest blood flow models only consider steady flow. However within the circulatory system, the periodic nature of the cardiac cycle induces a pulsatile, unsteady flow. This periodic pressure perturbation is expected to have significant implications for localised flow velocities and stress distributions.

We propose here a pulsatile flow model using a grid-free method, Smoothed Particle Hydrodynamics. This method is well suited to transient flows within geometries of complex shape. The arterial geometry used here is a real carotid bifurcation derived from MRI. Rigid walls and Newtonian flow are assumed. In this paper we compare pulsatile and steady flow for this geometry.

### **INTRODUCTION**

Blood flow is responsible for nutrient and waste transport within the closed-loop, cardiovascular network. Typically flow is laminar in healthy arteries, but the presence of abnormal flow conditions can promote the development of cardiovascular disease such as atherosclerosis and thrombus formation (excessive clotting).

The systemic flow is characterised predominantly by its pulsatile nature and the many levels of branching of the vascular network. The cyclic pumping of the heart periodically evacuates blood out of the ventricle and into the aorta generating a pressure pulse that propagates downstream through the arterial system. The combination of unsteady flow with certain features of geometry such as branch junctions, curved sections and flow constrictions can lead to complicated secondary flows incorporating flow separation, recirculation, stagnation and regions of high or low wall shear stress.

Local haemodynamics particularly in and around stenoses are believed to play an important role in cardiovascular disease. The likelihood of atherosclerotic plaque deposition is increased in regions of disturbed flow, but the relationship between fluid stresses and plaque growth is still not fully understood. Sawchuk et al (1994) and Zarinset et al. (1983) both found that plaque thickness depended on shear stress. Low wall shear stress (WSS) and flow velocity were observed where plaque thickness

was maximal. Conversely, plaque build-up was reduced where WSS and flow velocity were highest. The flow mechanism driving plaque growth is still uncertain and the rate of growth could depend on steady WSS; the shear stress gradient; or even an oscillating stress field.

Computational modelling of flow in diseased arteries using realistic geometries derived from Magnetic Resonance Imaging (MRI) is gaining favour as a tool for understanding and predicting cardiovascular disease (see Botnar et al. 2000, Prosi et al. 2004 and Marshall et al. 2004). This is because in vivo measurements of the flow field in an artery can be costly and are only possible for arteries that are easily accessible. Such measurements also provide very limited detail about the flow. Numerical models of arterial flow may provide researchers with a platform for testing how flow conditions can be modified in order to change or prevent disease.

Current CFD methods used for modelling of arterial flows rely on computing on a structured grid. Smoothed Particle Hydrodynamics (SPH) is a fully transient, Lagrangian CFD solver and does not use a grid. Instead computations are done on SPH 'particles' that travel with the flow carrying local state information with them. Boundary geometries of almost arbitrary complexity may be included such as artery walls. Since the boundaries also contain SPH particles, it is possible to make these walls elastic and compliant with the fluid stresses exerted on the walls. The advantage of SPH is that no re-meshing of the domain is required to model the wall deformations. Furthermore SPH particles carry local state information and can thus track fluid history easily. This, combined with the ability to modify particles according to a rule base, means that we can grow thrombotic protrusions into the flow and have them break off. We can then, in principle, follow this dangerous clot downstream into the cerebral vasculature. This is very hard in a traditional grid-based method and would enable investigation of critical medical problems well beyond the scope of traditional solvers. So the motivation for using SPH here, lies in the future deployment of the advantages described above.

In this study, we examine the differences between steady and pulsatile flow conditions for the flow field within a real, diseased, carotid artery bifurcation with rigid walls using the SPH method. The aim is to understand whether flow pulsatility is important for the development of cardiovascular disease in the carotid arteries; and as a prelude to looking at deformable walls interacting with the pulsatile flow.

## MODEL DESCRIPTION

### Smoothed Particle Hydrodynamics

The SPH methodology (Monaghan, 1992, 1994, 2005) consists of converting the partial differential equations encountered in fluid flow into algebraic equations. The interpolated value of a function  $A$  at any position  $\mathbf{r}$  can be expressed using SPH smoothing as:

$$A(\mathbf{r}) = \sum_b m_b \frac{A_b}{\rho_b} W(\mathbf{r} - \mathbf{r}_b, h) \quad (1)$$

Where  $m_b$  and  $\rho_b$  are the mass and density of particle  $b$  and the sum is over all particles  $b$  within a radius  $2h$  of  $\mathbf{r}$ . Here  $W(\mathbf{r}, h)$  is a  $C^2$  spline based interpolation or smoothing kernel with radius  $2h$  that approximates the shape of a Gaussian function. The gradient of the function  $A$  is given by differentiating the interpolation equation (1) to give:

$$\nabla A(\mathbf{r}) = \sum_b m_b \frac{A_b}{\rho_b} \nabla W(\mathbf{r} - \mathbf{r}_b, h) \quad (2)$$

Using these interpolation formulae and suitable finite difference approximations for second order derivatives, one is able to convert parabolic partial differential equations into ordinary differential equations for the motion of the particles and the rates of change of their properties.

From Monaghan (1992), the most suitable form of the SPH continuity equation is:

$$\frac{d\rho_a}{dt} = \sum_b m_b (\mathbf{v}_a - \mathbf{v}_b) \cdot \nabla W_{ab} \quad (3)$$

where  $\rho_a$  is the density of particle  $a$  with velocity  $\mathbf{v}_a$  and  $m_b$  is the mass of particle  $b$ . We denote the position vector from particle  $b$  to particle  $a$  by  $\mathbf{r}_{ab} = \mathbf{r}_a - \mathbf{r}_b$  and let  $W_{ab} = W(\mathbf{r}_{ab}, h)$  be the interpolation kernel with smoothing length  $h$  evaluated for the distance  $|\mathbf{r}_{ab}|$ . This form of the continuity equation is Galilean invariant (since the positions and velocities appear only as differences), has good numerical conservation properties and is not affected by free surfaces or density discontinuities.

The momentum equation can be written as:

$$\frac{d\mathbf{v}_a}{dt} = \mathbf{g} - \sum_b m_b \left[ \frac{\left( \frac{P_b}{\rho_b^2} + \frac{P_a}{\rho_a^2} \right)}{\mathbf{r}_a \mathbf{r}_b} - \frac{4\mathbf{m}_a \mathbf{m}_b}{(\mathbf{m}_a + \mathbf{m}_b) \rho_{ab}^2 + h^2} \frac{\mathbf{v}_{ab} \mathbf{r}_{ab}}{\rho_{ab}^2 + h^2} \right] \nabla_a W_{ab} \quad (4)$$

where  $P_a$  and  $\mu_a$  are pressure and fluid viscosity of particle  $a$  and  $\mathbf{v}_{ab} = \mathbf{v}_a - \mathbf{v}_b$ . Here  $\beta$  is a factor associated with the viscous term (Cleary 1996),  $\beta$  is a small parameter used to smooth out the singularity at  $\mathbf{r}_{ab}=0$  and  $\mathbf{g}$  is the gravity vector.

Since the SPH method used here is a quasi-compressible one needs to use an equation of state, giving the relationship between particle density and fluid pressure. A suitable one is:

$$P = P_0 \left[ \left( \frac{\rho}{\rho_0} \right)^\gamma - 1 \right] \quad (5)$$

where  $P_0$  is the magnitude of the pressure and  $\rho_0$  is the reference density. For water or blood we use  $\gamma = 7$ . This pressure is then used in the SPH momentum equation (3) to give the particle motion.

SPH formally resolves all length scales of the flow above the resolution length; much like a Large Eddy simulation. However, there is no formal turbulence modelling since the present SPH formulation does not have a sub-grid scale model.

### Carotid Arteries

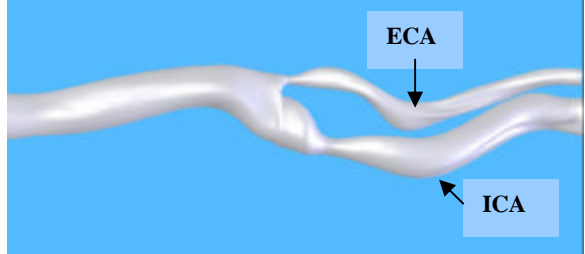


**Figure 1:** 3D model of real MRI derived arterial geometry of a diseased, carotid artery bifurcation. On the right, the upper daughter branch is the ECA and the lower branch is the ICA feeding blood to the brain.

The carotid arteries are located at the sides of the neck and supply blood to the face and brain. The common carotid artery (CCA) branches into the internal carotid artery (ICA), which feeds the brain, and the external artery (ECA), which transports blood to the muscles of the face and head.

Injury due to stroke arises from disease in the ICA manifesting itself as an arterosclerotic stenosed flow constriction. Complex flows immediately downstream from a stenosis are believed to be responsible for stresses leading to further plaque formation; or even plaque rupture which can lead to clotting at the stenosis. Furthermore ischemic stroke is a result of clot lodging in a blood vessel in the brain. It originates from places such as the carotid artery, aorta and heart.

Boundary conditions are required for the arterial flow simulations in this study. Figure 1 shows a real geometry of a diseased carotid artery derived from MRI (Beare et al., 2006). Raw surface geometry was extracted from a blocky, coarse resolution (1mm) MRI dataset. Spline based 2D profiles were fitted to the MRI voxel data and a solid geometry was constructed in the CAD package, Solidworks, by lofting between the 2D sections. A surface was extracted which represents the inner endothelial surface of the artery, and was then meshed with a commercial meshing package at a resolution of 0.5 mm.

An inflow velocity boundary condition was applied at the entrance of the CCA (to the left of Figure 1). For the steady case, a velocity of 0.15 m/s was chosen based on clinical measurements for this artery. Pulsatile conditions will be discussed in the next section. Outflow boundary conditions were also required to prevent the artery from draining and a constant pressure of 10 kPa was enforced at the exit points of the ICA and ECA arteries (to the right of Figure 1). Simulations commenced and the arteries were filled from the inflow until the arteries were fully pressurised as determined by measuring the pressures at the outflows.

### Pulsatile Flow Profile

Following each expulsion of blood from the heart and into the aorta, a pressure wave propagates downstream through the arterial system initiating local changes in pressure. These transients can significantly alter the flow field through the arteries. The flow field may also depend on wall elasticity and blood rheology, but these are often regarded as secondary effects relative to flow pulsatility. For the purposes of this study we have assumed the boundaries are rigid and that blood behaves as a Newtonian fluid.

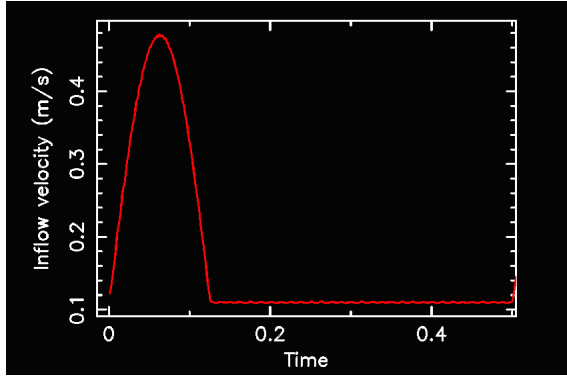


**Figure 2:** Pulsatile flow profile approximation used as a boundary condition for SPH simulation of pulsatile flow.

The physiological profile of a real pressure pulse at the entrance of the CCA depends on the cyclic pumping of the heart, the distensibility of the walls, and upstream and downstream pressures. During the diastolic phase of the heart when flow from the ventricle to the aorta is shut off, a non-zero flow through the arterial system is maintained as the elastic walls of the aorta contract.

We include pulsatile flow in the SPH simulation by imposing a time-varying velocity boundary condition at the entrance of the artery. As a first approximation to a physiological pulse, we use a sinusoidal profile. The shape of this pulse is given in Figure 2. The period used here is 0.5 s corresponding to a rapid heartbeat of 120 beats per minute (or 2 Hz), and the duration of the pulse is much shorter (just 0.125 s). The peak velocity is 0.5 m/s and the minimum is 0.1 m/s. A steady flow trailing the pulse represents the cut-off in supply from the heart during diastole. In a real pulse, there can be a degree of backflow during this time giving a small, negative pressure.

The Womersley number is a dimensionless parameter (similar to the Reynolds number) used specifically to characterise pulsatile flow within an artery. It is the ratio of inertial forces relative to viscous forces.

$$a = R \sqrt{\frac{2\pi f \rho}{\mu}} \quad (6)$$

where  $R$  is the radius of the artery,  $f$  is the pulsatile frequency,  $\rho = 1000 \text{ kg/m}^3$  has been used for fluid density, and  $\mu = 0.003 \text{ Pa s}$  is the dynamic viscosity. For the pulse described above in the common carotid artery of Figure 1 where the arterial diameter is 0.011 m, we obtain a Womersley number of 11, which is typical for this size artery. For large  $a$ , the flow becomes momentum dominated.

### RESULTS

Two cases have been simulated here for the same geometry artery: a steady flow, and a pulsatile flow.

#### **Passage of flow through the bifurcation**

To aid visualisation, SPH fluid particles were tagged periodically at the inflow to define a moving coherent band of fluid that could be tracked as it flowed through the artery. This band is shown in Figure 3 for the steady case at three different times, as it moves through the bifurcation. The SPH particles are shown here (and in the following figures) by a surface mesh surrounding them.

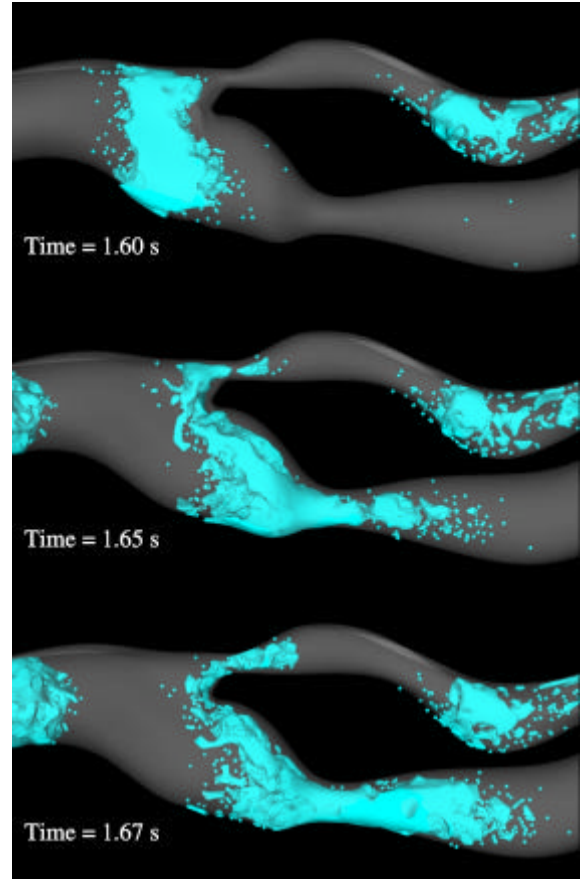


**Figure 3:** A band of fluid coloured blue is shown passing through the bifurcation at three different times.

Blood flows from the CCA up to the junction, before splitting into two separate flows into the daughter branches. Both the ICA and ECA branches are observed to have flow constrictions (stenoses) just past the junction.

The blue fluid band can be seen entering the branching junction at 1.6 s. An earlier band is visible in the top artery to the right. There is an asymmetry already in the band, with fluid moving forward into the carotid sinus in the bottom branch. The sinus is a characteristic enlarged region of the ICA just past the junction.

By 1.65 s, the flow is markedly split with the bulk of the fluid preferentially directed into the sinus. The narrow artery and mild flow constriction in the top artery, combined with the curved geometry leading up to the branching point, show only a small volume of fluid

entering the ECA. In the bottom ICA branch, fluid is accelerating into the stenosis.

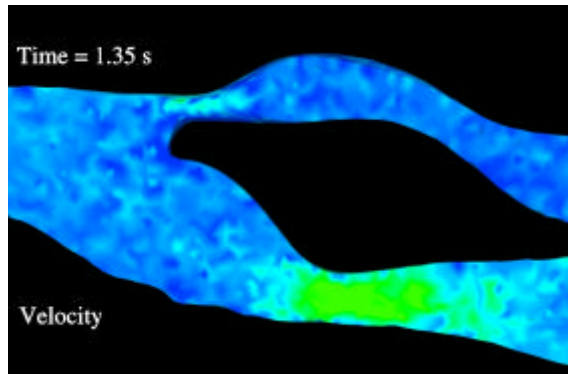


**Figure 4:** 3D clipped section of bifurcation for steady flow case showing the distribution of stream-wise velocities. Dark blue corresponds to 0.1 m/s (and greater) directed upstream, and red is 2.0 m/s (and greater) downstream.

ICA stenosis. Dark blue corresponds to 0.1 m/s (and greater) directed upstream, and red is 2.0 m/s (and greater) downstream.

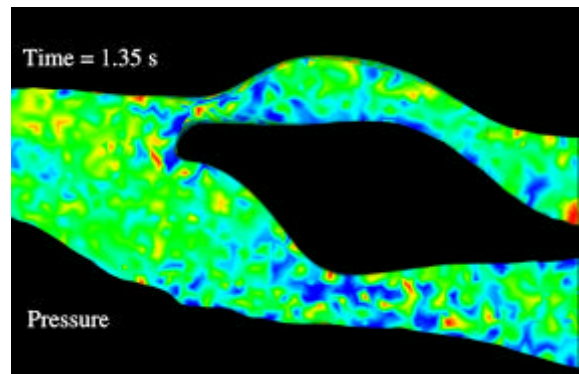


**Figure 6:** 3D clipped section of the bifurcation for steady flow case showing the distribution of pressure. Dark blue corresponds to 10 kPa (and lower), and red is 20 kPa (and greater).

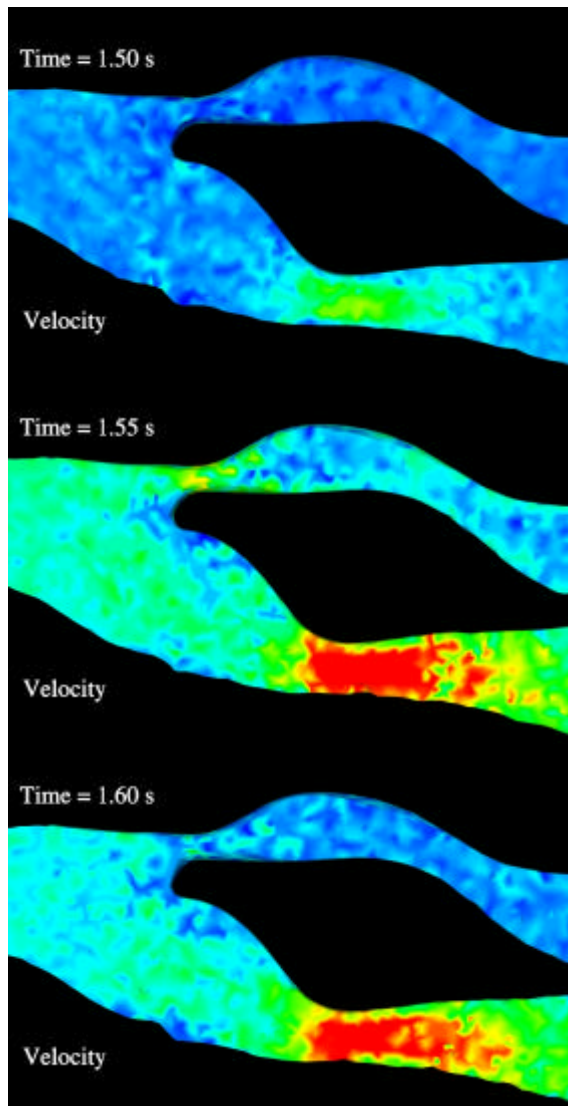


**Figure 5:** 3D clipped section of the bifurcation at 3 different times for the pulsed case showing the distribution of stream-wise velocities as the pulse travels through the

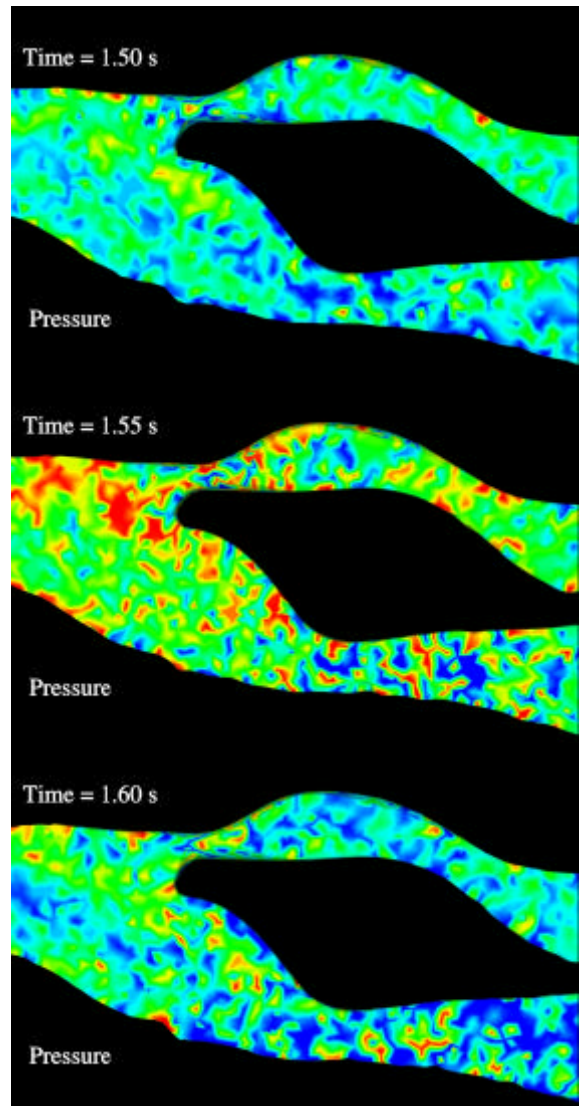


**Figure 7:** 3D clipped section of the bifurcation at 3 different times for the pulsed case showing the distribution

of pressure. Dark blue corresponds to 10 kPa (and lower), and red is 20 kPa (and greater).

The flow through the ICA stenosis is well underway by 1.67 s with an equal amount of fluid before and after the flow constriction. Significant drag on the fluid from the sinus walls is observed, while the fluid in the central region flows rapidly through the stenosis.

### Steady Flow vs Pulsatile Flow

The steady flow, coloured by stream-wise velocity and pressure respectively, is shown in Figures 4 and 6. Following the ICA branch, flow enters an enlarged section called the carotid sinus. Approaching the sinus the flow converges, increasing the pressure on the upstream side of the stenosis. Some backflow is observed on the walls of the sinus (see Figure 4) in trying to push too much volume through the stenosis. To maintain a constant volumetric flow rate through either the ECA or ICA stenosis, the flow necessarily accelerates as a narrow jet in the centre of the stenosis. These high velocities (up to 0.6 m/s for steady flow in the ICA constriction) generate a low pressure region within the stenosis as can be seen in Figure 6. For stenoses with near complete occlusion, a sufficient drop in pressure can result in closing the artery.

There is a drop in pressure visible across the ICA (see Figure 6) with more green fluid lying to the left of the stenosis and more blue to the right. This drives the high velocities through the stenosis. In the upper ECA branch, pressures look to be equalised across the stenosis with the downstream outflow pressure comparable to the pressure upstream of the stenosis. Limited flow occurs through this narrow artery and flow velocities appear to be very low downstream where the artery widens. Less blood supply is required for the face than for the brain; and hence the narrower artery. Since velocities in the ECA stenosis are smaller than in the ICA, and the volume of fluid is also less, any effects from secondary flows downstream from the stenosis will be limited. Thus there is typically less medical concern for disease build-up in this region.

We now consider the pulsatile case shown in Figures 5 and 7 coloured by velocity and pressure respectively. At 1.5 s, following the last pulse, the pressure has partially equalised across the lower ICA stenosis and the velocity is correspondingly reduced. As the next pulse reaches the stenosis (Figure 7 middle) pressures rise upstream, maximising the pressure difference across the stenosis. The flow accelerates (to around 2.5 m/s) through the stenosis until the downstream side achieves a pressure equivalent to that for the pressure drop for the steady case (Figure 7 bottom). The velocity then falls. As the pulse passes through the stenosis, the upstream pressure is relaxed and flow velocity decreases further until the downstream side once again pressurises.

### Sensor Readings

Pressure and velocity data is difficult to interpret quantitatively from 3D flow pictures and so we make use of virtual pressure sensors. A sensor was positioned in the stenosis of the ICA and measured time series data such as velocities and pressures in the local flow field.

The velocity and pressure histories in the ICA stenosis and near the inflow are reported here for the pulsatile flow case only. The velocity profiles near the inflow and at the stenosis are shown in Figure 8. The data is given for one period of the pulse. The velocity profiles are almost identical in shape, but the peak amplitude of the pulse in the stenosis is about 3.5 times greater than at the inflow and the minimum velocity is about 50% greater.

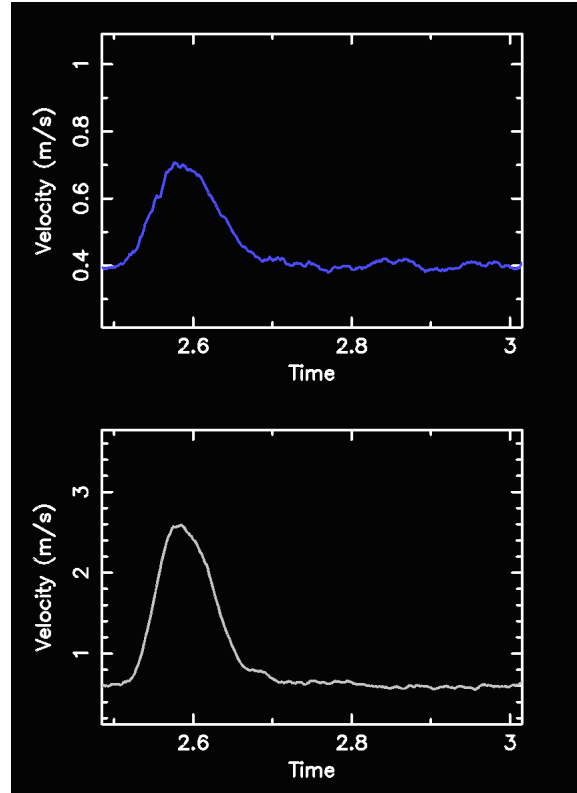


**Figure 8:** Velocity time series as measured for the pulsatile flow case near the inflow [top] and inside the ICA stenosis [bottom].

Pressure profiles are given in Figure 9. The pressure profile near the inflow corresponds to the shape of the velocity profile but with a small, constant offset in phase for all pulses. The pressure leads the velocity by 0.04 s (about 30 degrees).

Pressures within the stenosis are related to the inflow pressure but differ in profile. Near the inflow, the pulse peak pressure is reported as 23 kPa, and following the pulse the mean background pressure is 16 kPa. Reduced pressures of 17 kPa (peak) and 12 kPa (background) are found inside the stenosis as supported by the 3D flow pictures. The artery walls induce a drag in the flow, which creates a drop in the baseline pressure in the stenosis of about 25% relative to the inflow pressure. A non-trivial variation in pressure is observed in the stenosis for the duration of the pulse and appears to follow the velocity gradient of the pulse. The pressure appears to be high while the velocity is increasing, falls when the peak velocity is reached, and remains constant at a lower pressure than the baseline pressure while flow through the stenosis decelerates. Once the pulse has passed pressures then return to the baseline level.

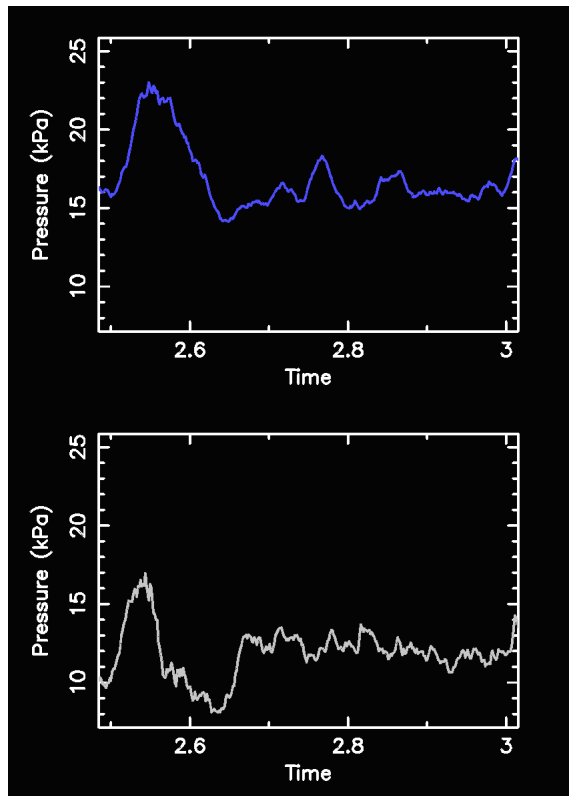


**Figure 9:** Pressure time series as measured for the pulsatile flow case near the inflow [top] and inside the ICA stenosis [bottom].

## CONCLUSION

We have studied the differences between steady and pulsatile flow behaviour in a stenosed carotid artery bifurcation using SPH simulations with a model pulse profile. Velocities and pressures have been analysed for the two cases using 3D flow pictures.

Steady flow appears to be preferentially directed into the internal carotid artery supplying blood to the brain. The external artery is narrow and only transports a relatively small volume for the same assumed downstream pressure as the internal artery. The stenosis in the internal carotid artery produces high velocities and low pressures with a well defined jet travelling from the centre of the sinus and through the centre of the stenosed region. Some drag is observed for blood adjacent to the sinus walls and perhaps even some backflow along the walls.

Pulsatile flow is responsible for an oscillation in pressure and velocity across the ICA stenosis. There is interplay between rising pressures at the stenosis and pressure equalisation across the stenosis that drives this oscillation. Velocities in the stenosis are very high for the pulsatile case and pressures are mildly reduced. The peak velocity for the pulsatile case is about 3.5 times that for the steady flow case but the peak pressure is reduced by 25% compared to the steady case.

The transient flow field from the pulsatile case has thus been shown to differ markedly from the steady case. The changes in pressure and velocity across the stenosis will

be important for understanding the local flow stresses leading to the development of cardiovascular disease.

## ACKNOWLEDGEMENTS

We gratefully acknowledge the support of Prof. Reutens' group from the Department of Medicine at Monash University in supplying the clinical geometry used in this study.

## REFERENCES

- BEARE, R., PHAN, T. and REUTENS, D., (2005), Department of Medicine, Monash University, Private Communication.
- BOTNAR, R., RAPPITSCH, G., SCHEIDEGGER, M.B., LIEPSCH, D., PERKTOLD, K. and BOESIGER, P., (2000), "Hemodynamics in the carotid artery bifurcation: a comparison between numerical simulations and in vitro MRI measurements", *J. Biomech.*, **33**, 137-144.
- CLEARY, P., (1996), "New implementation of viscosity: tests with Couette flows", *SPH Technical Note 8, CSIRO DMS, Technical Report DMS - C 96/32*.
- MARSHALL, I., ZHAO, S., HOSKINS, P., PAPATHANASOPOULOU, P. and YUN XU, X., (2004), "MRI and CFD studies of pulsatile flow in healthy and stenosed carotid bifurcation models", *J. Biomech.*, **37**, 679-687.
- MONAGHAN, J. J., (1992), "Smoothed Particle Hydrodynamics", *Ann. Rev. Astron. Astrophys.*, **30**, 543-574.
- MONAGHAN, J. J., (1994), "Simulating free surface flows with SPH", *J. Comp. Phys.*, **110**, 399-406.
- MONAGHAN, J. J., (2005), "Smoothed Particle Hydrodynamics", *Rep. Prog. Phys.*, **68**, 1703-1759.
- PROSI, M., PERKTOLD, K., DING, Z. and FRIEDMAN, M.H., (2004), "Influence of curvature dynamics on pulsatile coronary artery flow in a realistic bifurcation model", *J. Biomech.*, **37**, 1767-1775.
- SAWCHUK, A.P., UNTHANK, J.L., DAVIS, T.E. and DALRING, M.C., (1994), "A prospective, in vivo study of the relationship between blood flow haemodynamics and atherosclerosis in a hyperlipidemic swine model", *J. Vasc. Surgery*, **19**, 58-64.
- WOOTTON, D.M. and KU, D.N., (1999), "Fluid mechanics of vascular systems, diseases, and thrombosis", *Ann. Rev. Biomed. Eng.*, **1**, 299-329.
- ZARINS, C.K., GIDDENS, D.P. and BHARADAVAJ, B.K., (1983), "Carotid bifurcation atherosclerosis: quantification of plaque localization with flow velocity profiles and wall shear stress", *Circ. Research*, **53**, 502-514.